RSC Advances

ROYAL SOCIETY OF CHEMISTRY

www.rsc.org/advances

Journal Name RSCPublishing

ARTICLE

Novel Construction Technique, Structure and Photocatalysis of $Y_2O_2CN_2$ Nanofibers and Nanobelts

Cite this: DOI: 10.1039/x0xx00000x

Received 00th January 2012,
Accepted 00th January 2012

DOI: 10.1039/x0xx00000x

www.rsc.org/

Shan Xu, Xinlu Wang, Xiangting Dong*, Wensheng Yu, Jinxian Wang and Guixia Liu

Y_2O_3 nanofibers and nanobelts were fabricated by calcination of the respective electrospun PVP/$Y(NO_3)_3$ composite nanofibers and nanobelts. For the first time, $Y_2O_2CN_2$ nanofibers and nanobelts were successfully prepared via cyanamidation of the respective Y_2O_3 nanofibers and nanobelts employing NH_3 gas and using graphite boat as container at 950 °C. X-ray power diffraction (XRD) analysis reveals that $Y_2O_2CN_2$ nanofibers and nanobelts are pure trigonal phase with the space group of $P\bar{3}m1$. Scanning electron microscope (SEM) observation indicates that the diameter of $Y_2O_2CN_2$ nanofibers is 167.59±31.19 nm, and the thickness and width of $Y_2O_2CN_2$ nanobelts are respectively 154 nm and 2.02±0.84 μm under the 95 % confidence level. Fourier transform infrared spectroscopy (FTIR) analysis manifests that the trigonal $Y_2O_2CN_2$ nanofibers and nanobelts contain CN_2^{2-} ions. Brunauer-Emmett-Teller surface area (BET) measurement shows the surface areas of the $Y_2O_2CN_2$ nanofibers and nanobelts are 19.13 m^2/g and 15.92 m^2/g, respectively. $Y_2O_2CN_2$ nanostructures with different morphology exhibit high-efficiency photocatalytic capacity in photodegradation of rhodamine B (RhB) under the ultraviolet light irradiation, and the nanofibers have higher photocatalytic ability than nanobelts under the same experimental conditions. Furthermore, the nanofibers and nanobelts retain excellent photocatalytic stability after reused for four times. The photocatalytic mechanism and formation process of $Y_2O_2CN_2$ nanofibers and nanobelts are also provided.

1 Introduction

In recent years, rare-earth (RE) compounds have attracted much attention of the researchers due to their applications in permanent magnets, superconductors, catalysts and optical devices, etc [1-3]. There are many rare-earth compounds, such as RE_2O_2X (X=halogen, S^{2-}, Se^{2-}, Te^{2-}, CO_3^{2-} [4], CN_2^{2-} [5-6], SO_4^{2-} [7], etc), in which the crystal structure of the rare-earth compounds consists of $RE_2O_2^{2+}$ layers and their interleaving anion. Different kinds of anions can make structure, physical and chemical properties unique and multiple. A wide variety of function is anticipated by changing interlayer anions between $RE_2O_2^{2+}$ layers [6]. Research interest in C-N containing compounds of the lanthanides has been growing recently with the discovery of new $(N\text{-}C\text{-}N)^{2-}$ compounds such as $Eu(CN_2)$ [8], $LnCl(CN_2)N$ (Ln =La, Ce) [9], $La_2O(CN_2)_2$ [10] and $La_3Cl(CN_2)O_3$ [11].

Rare earth dioxymonocyanamides ($Ln_2O_2CN_2$) have become a very important family of the rare earth C-N containing compounds. The structure and composition of $La_2O_2CN_2$ powders were first reported by Hashimoto, et al [5].The linear anion $(N\text{-}C\text{-}N)^{2-}$ lies in parallel to the $La_2O_2^{2+}$ layers in structure because of the large ionic size of La^{3+}. The La^{3+} ions are coordinated with 4 oxygen and 4 nitrogen atoms in tetragonal lattice [5]. The $(N\text{-}C\text{-}N)^{2-}$ anions in $RE_2O_2CN_2$ are perpendicular with the smaller RE^{3+}, where RE= Y, Ce, Pr, Nd, Sm, Eu, Gd, Dy, Ho, Er, Tm, Yb). The RE^{3+} cations are coordinated with 4 oxygen and 3 nitrogen atoms in trigonal lattice [12-15].

All the homologous $Ln_2O_2(CN_2)$ Ln=Y, Ce-Gd, Dy-Yb [13-15] compounds were synthesized following the same procedure, solid-state metathesis (SSM) method or sol-gel method. For the first time, Xiaomin Guo with her co-workers successfully prepared tetragonal-phase $La_2O_2CN_2$ nanofibers and nanobelts, which were synthesized through cyanamidation technique of La_2O_3 respcetive nanostructures at high temperature employing NH_3 gas [16-19].

Nanofibers and nanobelts are new kinds of one-dimensional nanostructures with special morphologies. They have attracted increasing interest of scientists owing to their anisotropy, large length-to-diameter ratio and width-to-thickness ratio, unique optical, electrical and magnetic performances [20–26]. Therefore, study on the preparation and properties of nanofibers and nanobelts is still a popular subject in the field of materials science. Electrospinning is a simple, convenient, and versatile technique to prepare long fibers with diameters ranging from tens of nanometers up to micrometers, including yttrium oxysulfide nanofibers and nanobelts [26-27], rare-earth yttrium oxyfluoride hollow nanofibers and composite oxide nanofibers and nanobelts [20, 28-32]. However, to the best of our knowledge, there have been no reports on the preparation of Yttrium dioxymonocyanamides nanofibers and nanobelts by electrospinning combined with cyanamidation technique.

For Y, the ionic size (Y^{3+}=0.1015 nm) might be too small to stabilize the oxycyanamide in trigonal structure [6], so, it is hard

to prepare $Y_2O_2CN_2$, and there are only a few reports about the preparation and structure of $Y_2O_2CN_2$. Up to now, the fabrication of $Y_2O_2CN_2$ nanofibers and nanobelts is not reported in the literatures except for $Y_2O_2CN_2$ powders [13-14]. Herein, $Y_2O_2CN_2$ nanofibers and nanobelts were fabricated by cyanamidation of the relevant Y_2O_3 nanostructures which were prepared by calcination of the electrospun nanostructures of PVP/$Y(NO_3)_3$ composites in an ammonia atmosphere using graphite boat at high temperature. The morphology, structure and photocatalytic properties of the resulting samples were investigated in detail, and the formation mechanisms of $Y_2O_2CN_2$ nanostructures were also presented.

2 Experimental Sections

2.1 Chemicals

Polyvinyl pyrrolidone (Mw=90000, AR) were purchased from Tianjin Bodi Chemical Co., Ltd. *N,N*-dimethylformamide (DMF, AR) was bought from Tiantai Chemical Co., Ltd. Y_2O_3 (99.99%) was supplied by China Pharmaceutical Group Shanghai Chemical Reagent Company. Nitric acid (HNO_3, AR) was bought from Beijing Chemical Co., Ltd. NH_3 gas was supplied by Changchun Juyang Gas Co., Ltd. All chemicals were directly used as received without further purification.

2.2 Fabrication of $Y_2O_2CN_2$ nanofibers

Y_2O_3 nanofibers were prepared by calcining the electrospun PVP/$Y(NO_3)_3$ composite nanofibers. 1.0000 g of Y_2O_3 powers were dissolved in dilute (1:1, volume ratio) HNO_3 and evaporated to dryness by heating, then dissolved in 19.2347 g of DMF, and then 2.6782 g of PVP was added into the above solution under stirring for 8 h to form homogeneous transparent spinning solution. In the solution, the mass ratios of Yttrium nitrate, DMF and PVP were 10:79:11. Subsequently, PVP/$Y(NO_3)_3$ composite nanofibers were prepared by electrospinning technique. The spinning solution was electrospun at a positive high voltage of 13 kV, distance between the capillary tip and the collector was 18 cm, and relative humidity was 10 %-40 %. The collected electrospun composite nanofibers were then calcined at 700 °C in air for 8 h with the heating rate of 1 °C·min^{-1} to obtain Y_2O_3 nanofibers.
The Y_2O_3 nanofibers were loaded into a graphite boat and then heated to 950 °C at a heating rate of 1 °C·min^{-1} and remained for 12 h at 950 °C under a flow of gaseous ammonia. Then, the calcination temperature was decreased to 100 °C with a cooling rate of 1 °C·min^{-1}, followed by natural cooling down to room temperature, and $Y_2O_2CN_2$ nanofibers were successfully obtained.

2.3 Synthesis of $Y_2O_2CN_2$ nanobelts

Y_2O_3 nanobelts were prepared by calcining the electrospun PVP/$Y(NO_3)_3$ composite nanobelts. 1 g of Y_2O_3 were dissolved in dilute (1:1, volume ratio) HNO_3 and evaporated to dryness by heating, then dissolved in 17.0434 g DMF, and then 4.8695 g PVP was added into the above solution under stirring for 12 h to form homogeneous transparent spinning solution. In the spinning solution, the mass ratios of Yttrium nitrate, DMF and PVP were 10:70:20. Subsequently, PVP/$Y(NO_3)_3$ composite nanobelts were prepared by electrospinning technique. The spinning solution was electrospun at a positive high voltage of 8 kV, the distance between the capillary tip and the collector was 15 cm, and relative humidity was 40 %-60 %. The collected electrospun composite nanobelts were then calcined at 700 °C in air for 8 h at a heating rate of 1 °C·min^{-1} to acquire Y_2O_3 nanobelts.
$Y_2O_2CN_2$ nanobelts were fabricated through cyanamidation of the obtained Y_2O_3 nanobelts using the same process, as described in section 2.2.

2.4 Characterization methods

X-ray diffraction (XRD) analysis was performed using a Rigaku D/max-RA X-ray diffractometer with Cu kα radiation of 0.15406 nm. The size and morphology of the products were investigated by an XL-30 field emission scanning electron microscope (SEM) made by FEI Company. The purity of the products was examined by OXFORD ISIS-300 energy dispersive X-ray spectrometer (EDX). The specific surface areas of the nanostructures were measured by a V-Sorb 2800P specific surface area and pore size analyzer made by Gold APP Instrument Corporation. The samples were pre-evacuated for 120 min at 200 °C. Nitrogen gas is used as adsorption gas and adsorption process is carried out at 77 K applying nitrogen liquid as cooling agent. UV-Vis absorption spectra of the samples were taken with a UV-1240 spectrophotometer by Japanese Shimadzu Company. The Fourier transform infrared spectra of the samples were performed by a FTIR-8400S Fourier transform infrared spectrophotometer made by Shimadzu Corporation.

2.5 Evaluation of photocatalytic performance

In a typical photocatalytic reaction, 0.05 g of the as-prepared $Y_2O_2CN_2$ nanostructures were dispersed into a 100 mL aqueous solution of RhB with the concentration of 0.1 g·L^{-1}. Prior to illumination, the mixture was stirring for 1 h in the dark to make the nanostructures evenly disperse and reach adsorption-desorption balance in solution. Then the solution was exposed directly under the ultraviolet light (500 W ultraviolet lamp with main emission wavelength of 365 nm, FHSDI F6T5-365) with stirring to trigger decomposition of the RhB molecules. In a 20-minute interval, 4 mL suspension was sampled and centrifuged to remove the photocatalyst powders. The concentration of RhB aqueous solution was analyzed at maximum absorption of 553 nm, using a Shimadzu UV-1240 UV-Vis spectrophotometer. The degradation rate of RhB by $Y_2O_2CN_2$ nanostructures was estimated on the basis of the following formula [32]:

$$\eta = [(A_0 - A)/A_0] \times 100\%$$

where A_0 is the absorbance of RhB in the dark and A is the absorbance of Rh B at given time intervals after irradiation.
The stability of the $Y_2O_2CN_2$ nanostructures catalyst was evaluated by reusing the $Y_2O_2CN_2$ nanostructures catalyst for four runs for the decomposition of Rh B under the same conditions. After each run, the $Y_2O_2CN_2$ nanostructures catalyst were centrifugally separated, then washed for four times using distilled water, and then they were respectively reused. All the experiments were performed at room temperature.

3 Results and discussion

3.1 XRD analysis

Fig. 1 demonstrates the XRD patterns of the Y_2O_3 nanostructures. As seen from Fig. 1, the characteristic diffraction peaks of samples are observed in 2θ range of 10°–90°, which can be readily indexed to the cubic crystal phase of Y_2O_3 (PDF No. 25-1011).

As there is no PDF standard card of $Y_2O_2CN_2$, the phase composition of $Y_2O_2CN_2$ nanofibers and nanobelts is confirmed by comparing the XRD patterns of the $Y_2O_2CN_2$ products reported in the Ref. 13. Fig. 2 shows the XRD patterns of the as-prepared $Y_2O_2CN_2$ nanofibers and nanobelts. All the diffraction peaks are highly consistent those of the pure trigonal-phase of $Y_2O_2CN_2$ powders with space group of $P\bar{3}m1$ [13], and their structure comprises distinct covalent $Y_2O_2^{2+}$ complex cation and CN_2^{2-} anion layers. In this structure, the Y^{3+} ions are coordinated with four oxygen and three nitrogen atoms in trigonal lattice.

Obvious diffraction peaks are situated near 2θ = 10.08 º, 21.9 º, 27.96 º, 30.04 º, 35.98 º, 37.12 º, 43.74 º, 49.24 º, 50.54 º, 60.46 º, 80 º. No diffraction peaks of any other phases or impurities are detected, indicating that pure-phase $Y_2O_2CN_2$ nanostructures are successfully prepared.

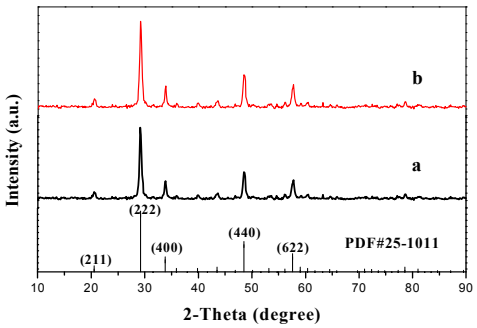

Fig. 1 XRD patterns of Y_2O_3 nanofibers (a) and Y_2O_3 nanobelts (b) with PDF standard card of Y_2O_3

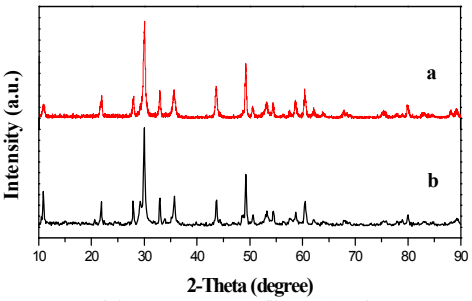

Fig. 2 XRD patterns of the $Y_2O_2CN_2$ nanofibers (a) and $Y_2O_2CN_2$ nanobelts (b)

3.2 Morphology observation

The morphologies of the products are characterized by scanning electron microscope (SEM). Fig. 3 manifests the representative SEM images of the composite nanofibers, composite nanobelts, $Y_2O_2CN_2$ nanofibers and $Y_2O_2CN_2$ nanobelts. From Fig. 3a, it can be noticed that the PVP/$Y(NO_3)_3$ composite nanofibers have smooth surface and uniform diameter. After annealing and cyanamidation at 950 °C, the diameter of the nanofibers greatly decreases due to loss of the PVP and associated organic components, as-formed $Y_2O_2CN_2$ nanofibers have relatively rough surface and uniform diameter ranging from 100 nm to 300 nm, as revealed in Fig. 3b. The SEM image of PVP/$Y(NO_3)_3$ composite nanobelts with the thickness of 492 nm (shown in the inset of Fig. 3c) is manifested in Fig. 3c, the composite nanobelts are relatively smooth and uniform and the seeming variation in width is mainly due to the twist of a nanobelt: the width, thickness and the twist parts of a nanobelt are simultaneously shown in a SEM image. The actual width of a single nanobelt is almost unchanged. The width value of a nanobelt is obtained by measuring the widest section of the nanobelt. Clearly, uniform $Y_2O_2CN_2$ nanobelts with the thickness of 154 nm (shown in the inset of Fig. 3d) are synthesized and have relatively rough surface, as indicates in Fig. 3d. Preliminarily, we can conclude that the cyanamidation plays an important role in keeping the morphology of the nanofibers and nanobelts.

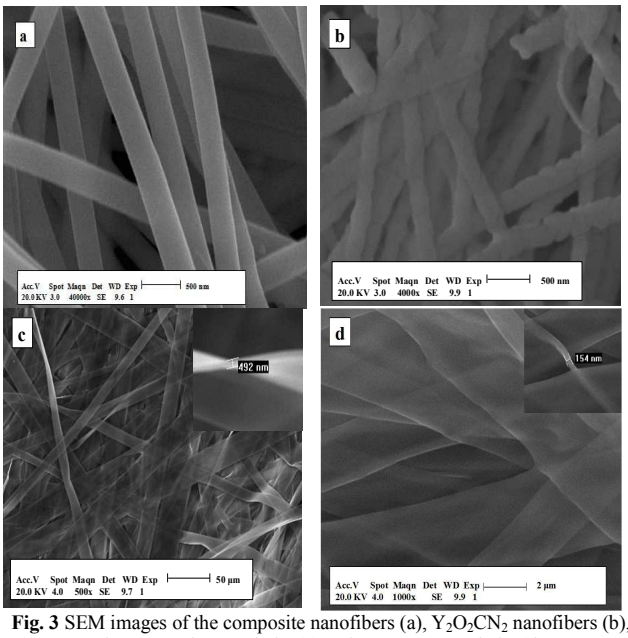

Fig. 3 SEM images of the composite nanofibers (a), $Y_2O_2CN_2$ nanofibers (b), the composite nanobelts (c) and $Y_2O_2CN_2$ nanobelts (d)

Under the 95% confidence level, the diameters of composite nanofibers and $Y_2O_2CN_2$ nanofibers, the width of composite nanobelts and $Y_2O_2CN_2$ nanobelts analyzed by Shapiro–Wilk method are normal distribution. Histograms of diameters and width of the nanostructures are indicated in Fig. 4. As seen from Fig. 4, the diameters of composite nanofibers, as-formed $Y_2O_2CN_2$ nanofibers, the width of composite nanobelts and $Y_2O_2CN_2$ nanobelts are 928.48±96.06 nm, 167.59±31.19 nm, 10.61±2.92 μm, and 2.02±0.84 μm, respectively.

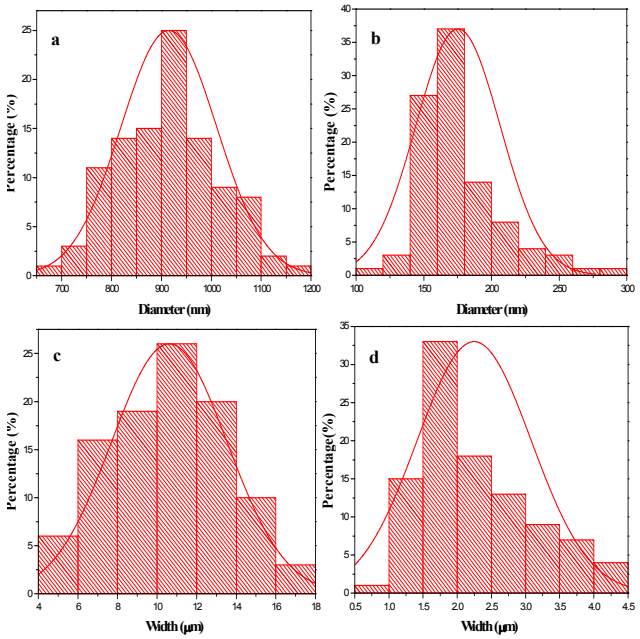

Fig. 4 Distribution histograms of diameter of the composite nanofibers (a), $Y_2O_2CN_2$ nanofibers (b), the width of the composite nanobelts (c) and $Y_2O_2CN_2$ nanobelts (d)

Fig. 5 demonstrates the EDX spectra of the PVP/$Y(NO_3)_3$ composites and $Y_2O_2CN_2$ nanostructures. EDX spectra analysis show that C, N, O and Y are the main elements in PVP/$Y(NO_3)_3$ composites and $Y_2O_2CN_2$ nanostructures. The content of C

element in $Y_2O_2CN_2$ nanostructures is much lower than that of the PVP/$Y(NO_3)_3$ composites due to the loss of the PVP and associate organic components. Au and Cr respectively come from the conductive films coated on the samples in preparation process for SEM analysis. No other elements are found in the samples, indicating that the $Y_2O_2CN_2$ nanostructures are highly pure.

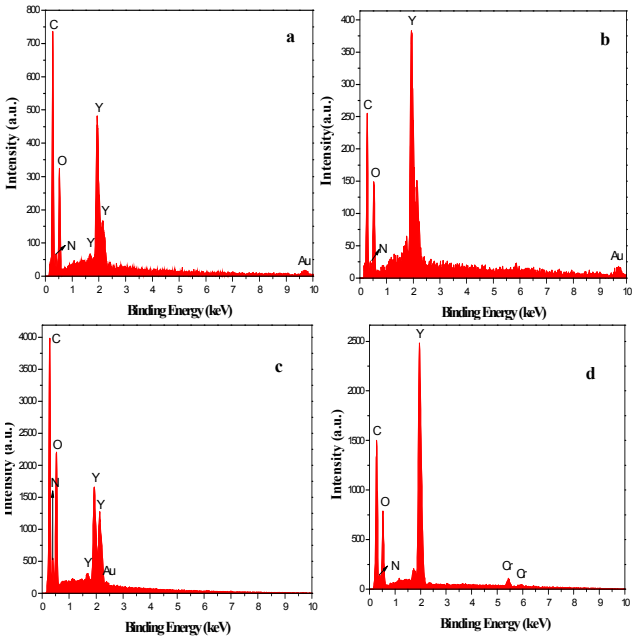

Fig. 5 EDX spectra of the composite nanofibers (a), $Y_2O_2CN_2$ nanofibers (b), the composite nanobelts (c) and $Y_2O_2CN_2$ nanobelts (d)

Fig. 6 respectively demonstrates the SEM image and elementary compositions of Y_2O_3 naonofibers. As reveals in Fig. 6(b), the energy dispersive spectra reveal the presence of Y, O, C and N elements in Y_2O_3 nanofibers. The element of Cr in the spectrum comes from the Cr film coated on the surface of the sample for SEM observation. No other elements are found in the samples, indicating that the Y_2O_3 naonofibers are highly pure.

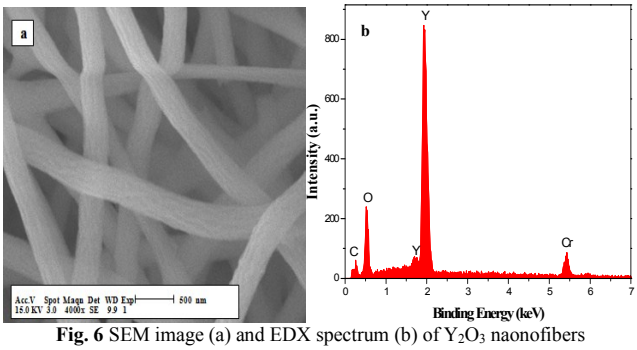

Fig. 6 SEM image (a) and EDX spectrum (b) of Y_2O_3 naonofibers

3.3 FTIR spectra

Fig. 7 shows the FTIR spectra of $Y_2O_2CN_2$ nanostructures, they all show two main absorption peaks in the vicinity of 654 cm^{-1} and 2141 cm^{-1}. These absorption peaks were assigned to the δ (formation vibration) and ν_{as} (antisymmetric stretch) modes of the CN_2^{2-} ions in $Y_2O_2CN_2$. The FTIR spectra of $Y_2O_2CN_2$ indicates that the trigonal $Y_2O_2CN_2$ nanofibers and nanobelts contain CN_2^{2-} ions [12].

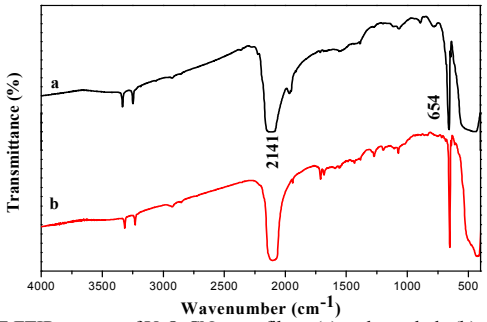

Fig. 7 FTIR spectra of $Y_2O_2CN_2$ nanofibers (a) and nanobelts(b)

3.4 UV–Vis absorption spectra

Fig. 8 reveals the UV–Vis absorption spectra of the $Y_2O_2CN_2$ nanofibers and nanobelts, the samples exhibit an intense absorption band in the range of 200–280 nm. It is well known that the optical absorption near the band edge for a direct transition crystalline semiconductor follows the formula [33-34]: $(\alpha h\nu)^{1/2}=B(h\nu-Eg)$. Where α, h, ν, Eg and B are absorption coefficient, Planck constant, light frequency, band gap and a constant, respectively. The typical Eg of $Y_2O_2CN_2$ nanofibers and nanobelts are respectively about 4.35 eV and 4.50 eV (the inset of Fig. 8; A is proportional to the absorption coefficient (α), α is substituted by A), which implies that the $Y_2O_2CN_2$ nanofibers and nanobelts could be used as ultraviolet light active photocatalyst.

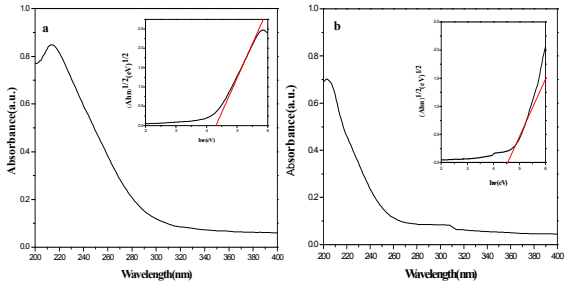

Fig. 8 UV–Vis absorption spectra of $Y_2O_2CN_2$ nanofibers (a) and nanobelts (b)

3.5 Specific surface area analysis

The specific surface area of the $Y_2O_2CN_2$ nanofibers and nanobelts were determined by BET method. The measured BET surface area adsorption-desorption isotherms of $Y_2O_2CN_2$ samples are indicated in Fig. 9. The P/P_0 ranges of $Y_2O_2CN_2$ nanofibers and nanobelts were respectively 0.0120-0.3251 and 0.0097-0.3144. We conclude that the monolayer adsorption saturation capacity of nanofibers and nanobelts, which are obtained respectively from the inset of Fig. 9, are 2.37 mL and 2.81 mL. The BET model surface areas are calculated in the following formula:

$$BET= [(V_m\times10^{-3})/22.4] \times6.02\times10^{23}\times1.62\times10^{-19}$$

The BET model surface areas of the $Y_2O_2CN_2$ nanofibers and nanobelts are calculated to be 19.13 m^2/g and 15.92 m^2/g respectively. Remarkably, the specific surface area of the $Y_2O_2CN_2$ nanofibers is bigger than that of the $Y_2O_2CN_2$ nanobelts.

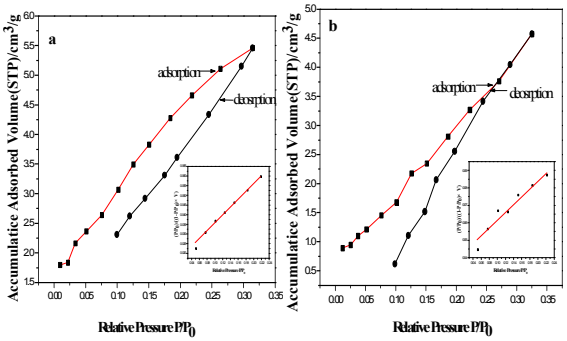

Fig. 9 BET surface area adsorption isotherms of $Y_2O_2CN_2$ nanofibers (a) and nanobelts (b)

3.6 Photocatalysis

The photocatalytic activity of the $Y_2O_2CN_2$ nanofibers and nanobelts were evaluated by the degradation of RhB aqueous solution under ultraviolet irradiation, as indicated in Fig. 10. Fig. 10a displays the absorption spectra of the RhB aqueous solution during the photocatalytic degradation process by the $Y_2O_2CN_2$ nanofibers catalyst. The absorption spectra of RhB at λ_{max} = 553 nm decrease gradually after photocatalytic reaction for 180 min, implying that the chromophoric groups of RhB molecules have been destroyed, and the degradation rates of RhB by $Y_2O_2CN_2$ nanofibers and the $Y_2O_2CN_2$ nanobelts were respectively 99.50 % and 94.90 %, as shown in Fig. 10a and Fig. 10b. Fig. 10c displays the degradation curves of RhB for the nanofibers and nanobelts at the first run. The rate constants for the degradation experiments are determined to be 0.0272 and 0.0165 for $Y_2O_2CN_2$ nanofibers and nanobelts, respectively. The $Y_2O_2CN_2$ nanofibers exhibit higher photocatalytic activities than the nanobelts from the beginning to the end, which is attributed to the fact that the BET surface area of nanofibers is bigger than that of the nanobelts. In order to confirm the stability of the photocatalytic performance of the $Y_2O_2CN_2$ nanomaterials catalyst, the circulating runs in the photocatalytic degradation of RhB in the presence of $Y_2O_2CN_2$ nanofibers and nanobelts catalysts under ultraviolet light are carried out, as shown in Fig. 11. After four recycles for the photocatalytic degradation of RhB, the catalysts do not exhibit significant loss of photocatalytic activity.

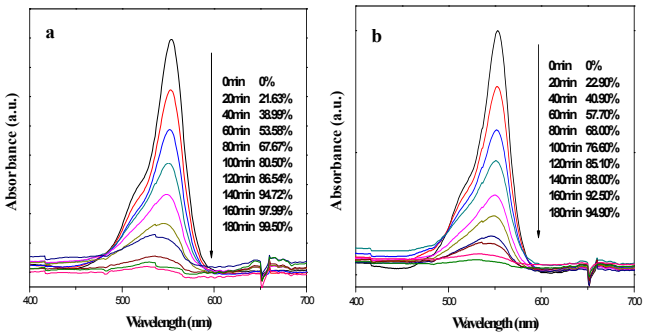

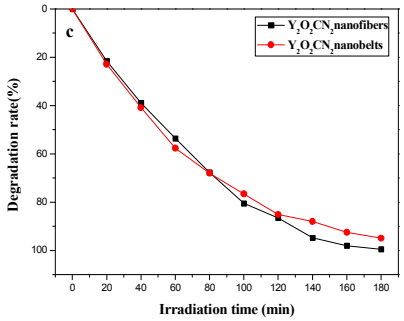

Fig. 10 Absorption spectra variation of RhB at different reaction time for $Y_2O_2CN_2$ nanofibers (a) and $Y_2O_2CN_2$ nanobelts (b), and the degradation curve of RhB over sample $Y_2O_2CN_2$ nanomaterials (c)

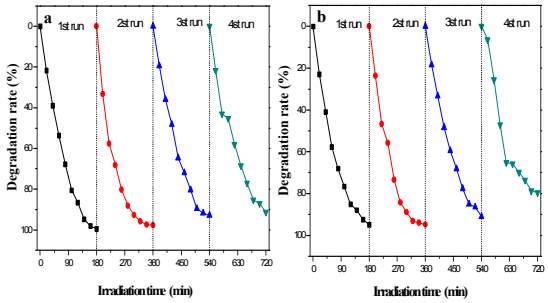

Fig. 11 Degradation curves of RhB over sample $Y_2O_2CN_2$ nanofibers (a) and nanobelts (b)

Fig. 12 shows the first order reaction rate equation of the degradation experiments for $Y_2O_2CN_2$ nanofibers and $Y_2O_2CN_2$ nanobelts. The rate constants are determined to be 0.01685 min^{-1} and 0.01555 min^{-1} for $Y_2O_2CN_2$ nanofibers and nanobelts.

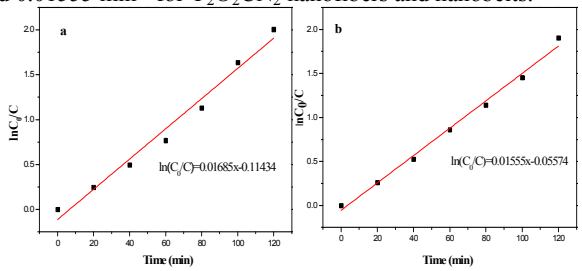

Fig. 12 The first order reaction rate curve and equation of the degradation experiments for $Y_2O_2CN_2$ nanofibers (a) and $Y_2O_2CN_2$ nanobelts (b)

3.7 Possible mechanism of the ultraviolet-induced photodegradation of RhB

Based on the above results, a possible photocatalytic mechanism is indicated in Fig. 13. As shown in Fig. 13, $Y_2O_2CN_2$ with narrow band gap energy (Eg of nanofibers and nanobelts are respectively about 4.35 eV and 4.50 eV) could be easily excited by ultraviolet light and the generation of photoelectrons and holes is induced. Then the photo-generated electrons (e^-) probably react with dissolved oxygen molecules to yield super oxide radical anions, O_2^-, which on protonation generated the hydroperoxy, $HO_2^{\cdot}$, radicals, producing the hydroxyl radical $OH^{\cdot}$, which is a strong oxidizing agent, to decompose the organic dye. [35–40]. A hypothetical mechanism is proposed for the photocatalytic degradation of RhB as follows:

$$Y_2O_2CN_2 + h\nu \longrightarrow Y_2O_2CN_2(e^- + h^+) \quad (1)$$

$$Y_2O_2CN_2(e^-) + O_2 \longrightarrow Y_2O_2CN_2 + O_2^- \quad (2)$$

$$O_2^- + H_2O \longrightarrow HO_2^{\cdot} + OH^- \quad (3)$$

$$HO_2^{\cdot} + H_2O \longrightarrow H_2O_2 + OH^{\cdot} \quad (4)$$

$$H_2O_2 \longrightarrow 2OH^{\cdot} \quad (5)$$

$$Y_2O_2CN_2(h^+) + H_2O + OH^- \longrightarrow Y_2O_2CN_2 + 2OH^{\cdot} \quad (6)$$

$$OH^{\cdot} + RhB \longrightarrow \text{degraded or mineralized products} \quad (7)$$

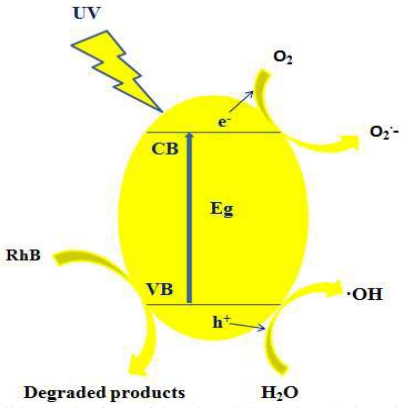

Fig 13 Possible mechanism of the ultraviolet-induced photodegradation of RhB with $Y_2O_2CN_2$ nanofibers and nanobelts

4 Formation mechanism for $Y_2O_2CN_2$ nanostructures

According to the above analysis, we advance the formation mechanism of $Y_2O_2CN_2$ nanostructures, as shown in Fig. 14. PVP and $Y(NO_3)_3$ are mixed with DMF to form spinning solution. PVP act as template during the formation of $Y_2O_2CN_2$ nanostructures. Y^{3+} and NO_3^- are mixed or absorbed onto PVP to form PVP/$Y(NO_3)_3$ composite nanofibers and nanobelts via electrospinning. Some solvents are volatilized in the electrospinning process. PVP decompose soon and carbonize, nitrates are decomposed and oxidized to produce NO_2, and eventually evaporate from the composite fibers and belts during calcinations process. With the increase in the calcining temperature, Y^{3+} could combine with O_2, coming from air, to form Y_2O_3 crystallite, and many crystallites are combined into nanoparticles, and finally these nanoparticles mutually connect to generate Y_2O_3 nanofibers and nanobelts. Afterwards, the above products are cyanamidated in a graphite boat under the flowing NH_3. In the cyanamidation process, the graphite from graphite boat reacts with the flowing ammonia gas and Y_2O_3 to produce $Y_2O_2CN_2$, CO and H_2 in the high temperature. During the process, graphite boat is not only a container, but also a reactant substance through reacting with NH_3 and Y_2O_3 in the heating process. Cyanamidation technology we proposed here is actually a solid–gas reaction, which has been proved to be an important method, not only can retain the morphology of precursor, but also can fabricate pure phase $Y_2O_2CN_2$ nanostructures. Reaction schemes for formation of $Y_2O_2CN_2$ nanostructures proceed as follows:

$$PVP/Y(NO_3)_3 + O_2 \xrightarrow{700\ ^\circ C} CO_2 + H_2O + NO_2 + Y_2O_3 \quad (8)$$

$$NH_3 + C \xrightarrow{950\ ^\circ C} H_2CN_2 + 2H_2 \quad (9)$$

$$Y_2O_3 + H_2CN_2 + C \xrightarrow{950\ ^\circ C} Y_2O_2CN_2 + CO + H_2 \quad (10)$$

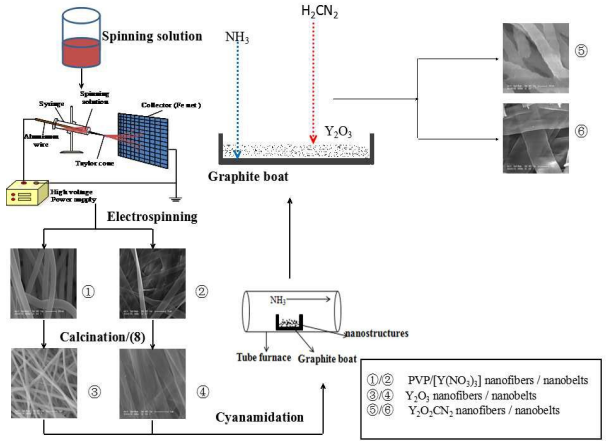

Fig. 14 Schematic diagram of formation mechanism of $Y_2O_2CN_2$ nanofibers and nanobelts

5 Conclusions

In summary, for the first time, pure trigonal phase $Y_2O_2CN_2$ nanofibers and nanobelts with space group of $P\bar{3}m1$ have been successfully prepared by electrospinning in conjunction with cyanamidation technology using NH_3 gas and graphite at high temperature. The as-prepared $Y_2O_2CN_2$ nanostructures have relatively rough surface, the diameter of the nanofibers is 167.59±31.19 nm, the width of nanobelts is 2.02±0.84 μm. $Y_2O_2CN_2$ nanofibers and nanobelts possess excellent photocatalytic performance and their photocatalytic effects are stable. The cyanamidation technology we proposed here is of great importance, it can be applicable to the synthesis of other homologous rare earth oxycyanamide nanostructures with various morphologies such as $Y_2O_2CN_2$:RE^{3+} and $Ln_2O_2CN_2$:RE^{3+} (Ln=Pr, Nd, Gd, etc).

Acknowledgments

This work was financially supported by the National Natural Science Foundation of China (51573023, 50972020, 51072026), Ph.D. Programs Foundation of the Ministry of Education of China (20102216110002,20112216120003), the Science and Technology Development Planning Project of Jilin Province (Grant Nos. 20130101001JC, 20070402).

Notes and references

Key Laboratory of Applied Chemistry and Nanotechnology at Universities of Jilin Province, Changchun University of Science and Technology, Changchun 130022. Fax: 86 0431 85383815; Tel: 86 0431 85582574; E-mail: dongxiangting888@163.com

[1] M. Li, W. X. Yuan, J. F. Wang, and C. Gu, *Powder Diffr.*, 2007, 22, 59-63.
[2] S. Q. Su, W. Chen, C. Qin, S. Y. Song, Z. Y. Guo, G. H. Li, X. Z. Song, M. Zhu, S. Wang, Z. M. Hao and H. J. Zhang, *Cryst. Growth Des.*, 2012, 12, 1808-1815.
[3] J. B. Yu, L. Zhou, H. J. Zhang, Y. X. Zheng, H. R. Li, R. P. Deng, Z. P. Peng and Z. F. Li, *Inorg. Chem.*, 2005, 44, 1611-1618.
[4] G. G. Li, C. Peng, C. M. Zhang, Z. H. Xu, M. M. Shang, D. M. Yang, X. J. Kang, W. X. Wang, C. X. Li, Z. Y. Cheng, and J. Lin, *Inorg. Chem.*, 2010, 49, 10522-10535.
[5] Y. Hashimoto, M. Takahashi, S. Kikkawa and F. Kanamaru, *J. Solid State Chem.*, 1995, 114, 592-594.
[6] T. Takeda, N. Hatta, and S. Kikkawa, *Chem. Lett.*, 2006, 35, 988-989.
[7] M. Machida, K. Kawamura and K. Ito, *ChemInform*, 2004, 35, 662-663.
[8] O. Reckeweg and F. J. DiSalvo, *Z. Anorg. Allg. Chem.*, 2003, 629, 177-179.

[9] R. Srinivasan, M. Ströbele and H.-J. Meyer, *Inorg. Chem.*, 2003, 42, 3406-3411.
[10] R. Srinivasan, S. Tragl, and H.-J. Meyer, *Z. Anorg. Allg. Chem.*, 2005, 631, 719-722.
[11] M. Kubus, D. Enseling, T. Justel, and H.-J. Meyer, *Eur. J. Inorg. Chem.*, 2013, 2013, 3195-3199.
[12] Y. Hashimoto, M. Takahashi, S. Kikkawa and F. Kanamaru, *J. Solid State Chem.*, 1996, 125, 37-42.
[13] J. Sindlinger, J. Glaser, H. Bettentrup, T. Jüstel and H.-J. Meyer, *Z. Anorg. Allg. Chem.*, 2007,633, 1686-1690.
[14] M. Zeuner, S. Pagano and W. Schnick, *Chemistry*, 2008, 14, 1524-1531.
[15] S. Pagano, M. Zeuner, U. Baisch and W. Schnick, *Z. Anorg. Allg. Chem.*, 2010, 636, 2212-2221.
[16] X. M. Guo, X. T. Dong, J. X. Wang, W. S. Yu and G. X. Liu, *Chem. Eng. J.*, 2014, 50, 148-156.
[17] X. M. Guo, W. S. Yu , X. T. Dong, J. X. Wang, Q. L. Ma, G. X. Liu and M. Yang, *J. Am. Ceram. Soc.*, 2015, 98, 1215-1222.
[18] X. M. Guo, J. X. Wang, X. T. Dong, W. S. Yu and G. X. Liu, *CrystEngComm*, 2014, 16, 5409.
[19] X. M. Guo, W. S. Yu, X. T. Dong, J. X. Wang, Q. L. Ma, G. X. Liu and M. Yang, *Eur. J. Inorg. Chem.*, 2015(3), 389-396.
[20] J. X. Wang, H. R. Che, X. T. Dong, L. Liu, G. X. Liu, *Acta Opt. Sinica*, 2010, 30, 473–479.
[21] Q. Z. Cui, X. T. Dong, J. X. Wang and M. Li, *J. Rare Earths*, 2008, 26, 664–669.
[22] L. Y. Yang, J. X. Wang, X. T. Dong, G. X. Liu and W. S. Yu, *J. Mater. Sci.*, 2013, 48, 644–650.
[23] Q. L. Ma, J. X. Wang, X. T. Dong, W. S. Yu and G. X. Liu, *Chem. Eng. J.*, 2013, 222, 16–22.
[24] W. W Ma, X. T. Dong, J. X. Wang, W. S. Yu and G. X. Liu, *J. Mater. Sci.*, 2013, 48, 2557–2565.
[25] Q. L. Ma, J. X. Wang, X. T. Dong, W. S. Yu, G. X. Liu and J. Xu, *J. Mater. Chem.*, 2012, 22, 14438–14442.
[26] H. Y. Wang, Y. Yang, Y. Wang, Y. Y. Zhao, X. Li and C. Wang, *J. Nanosci. Nanotechnol.*, 2009, 9, 1522–1525.
[27] X. Lu, M. Yang, L. Y. Yang, Q. L. Ma, X. T. Dong and J. Tian, *J. Mater. Sci. - Mater. Electron.*, 2015, 26, 4078-4084.
[28] Y. Liu , J. X. Wang, X. T. Dong and G. X. Liu, *Chem. J. Chin. Univ.*, 2010, 31, 1291–1296.
[29] X. T. Dong, L. Liu, J. X. Wang and G. X. Liu, *Chem. J. Chin. Univ.*, 2010, 3, 20–25.
[30] D. Li, W. S. Yu, X. T. Dong, J. X. Wan and G. X. Liu, *J. Fluorine Chem.*, 2013, 145, 70-76.
[31] D. Li, X. T. Dong, W. S. Yu, X. Wan and G. X. Liu, *J. Mater. Sci. - Mater. Electron.*, 2013, 24, 3041-3048.
[32] J. X. Wang, Y. Q. Guo, X. T. Dong, Z. G. Li and G. X. Liu, *J. Inorg. Mater.*, 2010, 25, 379–385.
[33] Y. C. Chou, C. L. Shao, X. H. Li, C. Y. Su, H. C. Xu, M. Y. Zhang, P. Zhang, X. Zhang and Y. C. Liu, *Appl. Surf. Sci.*, 2013, 285, 509–516.
[34] C. H. Wang, C. L. Shao, Y. C. Liu, X. H. Li. *Inorg. Chem.,* 2009, **48**, 1105-1113.
[35] Z. Y. Zhang, C. L. Shao, X. H. Li, Y. Y. Sun, M. Y. Zhang, J. B. Mu, P. Zhang, Z. C. Guo and Y. C. Liu, *Nanoscale*, 2013, 5, 606–618.
[36] M. Y. Zhang, C. L. Shao, J. B. Mu, X. M. Huang, Z. Y. Zhang, Z. C. Guo, P. Zhang and Y. C. Liu, *J. Mater. Chem.*, 2012, 22, 577.
[37] M. Y. Zhang, C. L. Shao, P. Zhang, C. Y. Su, X. Zhang, P. P. Liang, Y. Y. Sun and Y. C. Liu, *J. Hazard. Mater.*, 2012, 225–226, 155–163.
[38] M. Y. Zhang, C. L. Shao, Z. C. Guo, Z. Y. Zhang, J. B. Mu, T. P. Cao and Y. C. Liu, *ACS Appl. Mater. Interfaces*, 2011, 3, 369–377.
[39] P. Zhang, X. H. Li, C. L. Shao and Y. C. Liu, *J. Mater. Chem. A*, 2015, 3, 3281-3284.
[40] M. Y. Zhang, C. L. Shao, X. Zhang and Y. C. Liu, *CrystEngComm*, 2015, 17, 7276-7282.

Graphical Abstract

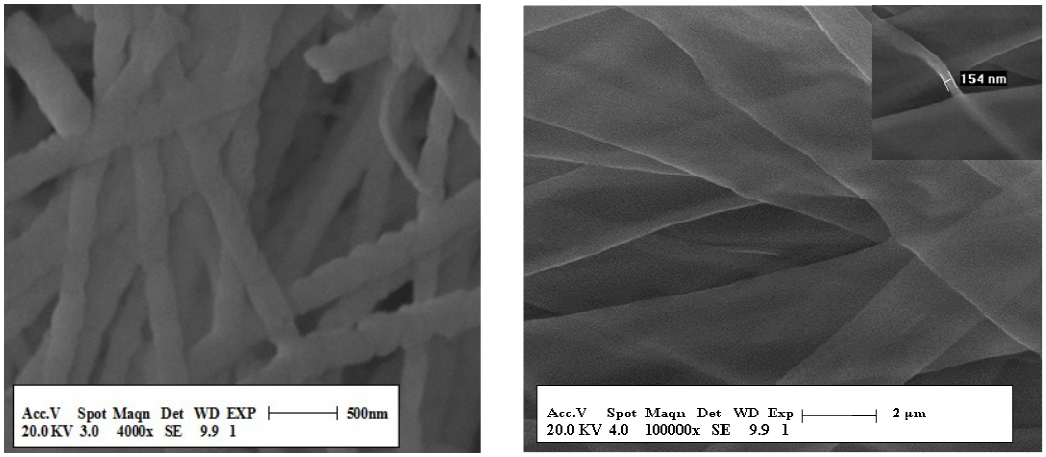

Pure trigonal phase $Y_2O_2CN_2$ nanofibers and nanobelts have been successfully prepared by electrospinning in conjunction with cyanamidation technology. $Y_2O_2CN_2$ nanofibers and nanobelts possess excellent and stable photocatalytic performance. The cyanamidation technology we proposed here is of great importance to fabricate other homologous rare earth oxycyanamide nanostructures with various morphologies.